Mark Berlin

Predicting Oral Absorption of Poorly Soluble Weakly Basic Drugs

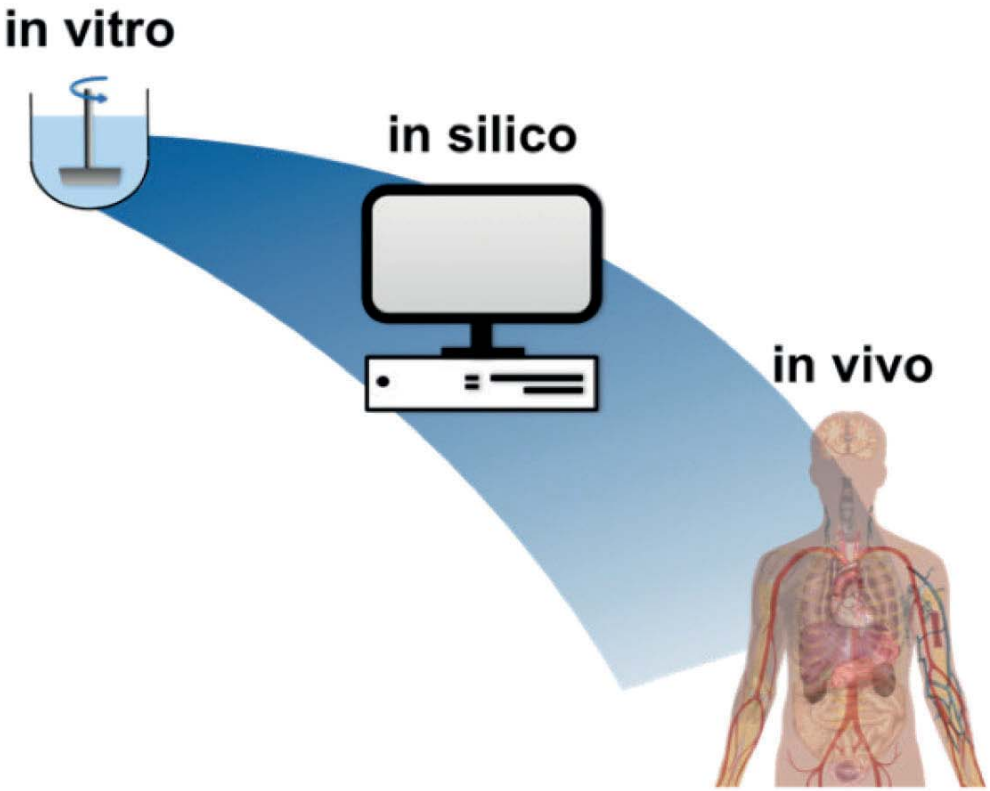

Cuvillier Verlag Göttingen
Internationaler wissenschaftlicher Fachverlag

Predicting Oral Absorption of Poorly Soluble Weakly Basic Drugs

Mark Berlin

Predicting Oral Absorption of Poorly Soluble Weakly Basic Drugs

Cuvillier Verlag Göttingen
Internationaler wissenschaftlicher Fachverlag

Bibliografische Information der Deutschen Nationalbibliothek
Die Deutsche Nationalbibliothek verzeichnet diese Publikation in der Deutschen Nationalbibliografie; detaillierte bibliografische Daten sind im Internet über http://dnb.d-nb.de abrufbar.
1. Aufl. - Göttingen: Cuvillier, 2015
Zugl.: Frankfurt am Main, Univ., Diss., 2015

Nonnenstieg 8, 37075 Göttingen
Telefon: 0551-54724-0
Telefax: 0551-54724-21
www.cuvillier.de

1. Auflage, 2015
Gedruckt auf umweltfreundlichem, säurefreiem Papier aus nachhaltiger Forstwirtschaft.

ISBN 978-3-7369-9146-0
eISBN 978-3-7369-8146-1

Acknowledgements

First and foremost my deepest gratitude to Prof. Dr. Jennifer B. Dressman for her continuous guidance, support and encouragement throughout my research work. I want to thank for her time and energy invested in valuable advices, discussions as well as for her admirable care, motivation and open mindedness. I deeply appreciate being given the opportunity to work under the supervision of Prof. Dressman.

I also want to thank my friends and colleagues at the Institute of Pharmaceutical Technology, namely Mr. Cord Andreas, Dr. Marcel Arndt, Ms. Susanne Bayer, Ms. Gerlinde Born, Dr. Miriam Dadparvar, Mr. Yang Fei, Mr. Alexander Fuchs, Ms. Simone Hansmann, Mrs. Christine Janas, Dr. Atsushi Kambayashi, Dr. Murat Kilic, Mr. Andeas Koczwara, Dr. Edmund “Ed” Kostewicz, Prof. Dr. Jörg Kreuter, Dr. Anna Christine Mieden, Dr. Astrid Mühlstein, Ms. Lisa Nothnagel, Mr. Keiichi Otsuka, Dr. Ina Rosenberger, Mr. Karim Sempf, Dr. Thomas Taupitz, Mr. Julian Thinnes, Dr. Waralee Watcharin, Dr. Matthias Wacker and Dr. Christian Wagner.
My very special thanks go to Dr. Anita Nair, Dr. Stefanie Straub and Mr. Aaron Ruff for the good times we had.
My appreciation goes also to the technical staff of the Institute, Mrs. Hannelore Berger, Ms. Mareike Götz, Mrs. Elisabeth “Sissy” Herbert, Mrs. Birgit Johann, Mr. Kaufmann and Mrs. Sylvia Niederdorf.

Big thanks go to our project partners, Dr. Dieter Baumann, Mr. Karl-Heinz Przyklenk, Mrs. Annette Richtberg (Hennig Arzneimittel GmbH, Flörsheim am Main, Germany), Dr. Filippos Kesisoglou, Mr. Michael Hong Wang and Mrs. Wei Xu (Merck Sharp & Dohme, Kenilworth, New Jersey, USA) for their professional support, valuable discussions and input. Special thanks go also to Prof. Dr. Christos Reppas (National and Kapodistrian University, Athens, Greece) for the valued scientific input and conversations.

My deepest gratitude, appreciation and love go to my dear parents, Henrietta Deborah Ruth and Alexander and to my dear sister Beata Esther Feiga for their incomparable encouragement and motivation throughout my studies and PhD work. Without you it would not have been possible.

Dedicated to my parents,

Henrietta Deborah Ruth and Alexander Berlin

“Stay hungry. Stay foolish.”
Steward Brand

Predicting Oral Absorption of Poorly Soluble Weakly Basic Drugs

Dissertation
zur Erlangung des Doktorgrades
der Naturwissenschaften

Vorgelegt beim Fachbereich 14
Biochemie, Chemie und Pharmazie
der Goethe-Universität
in Frankfurt am Main

von Mark Berlin
aus Vilnius (Litauen)

Frankfurt am Main, 2015
(D30)

vom Fachbereich der Biochemie, Chemie und Pharmazie der Goethe-Universität als Dissertation angenommen.

Dekan: Prof. Dr. Michael Karas

1. Gutachter: Prof. Dr. Jennifer B. Dressman
2. Gutachter: Prof. Dr. Christos Reppas

Datum der Disputation: 11. November 2015

Index

1 Introduction 1

1.1 Drug transit through the upper GI tract 2

1.2 Determinants of drug absorption 4

1.2.1 The biopharmaceutics classification system 4

1.2.2 The biopharmaceutics drug disposition classification system 5

1.2.3 The developability classification system 6

1.3 Weak bases and the GI tract 7

1.3.1 pH in the GI tract 7

1.3.2 Bile salts and food in the GI tract 9

1.3.3 Gastric emptying 10

1.4 Simulation of *in vivo* drug dissolution 10

1.4.1 Dissolution media simulating GI fluids 10

1.4.2 Simulation of GI dissolution conditions 11

1.5 Drug permeability assessment 14

1.6 Physiologically based pharmacokinetic modeling 16

1.6.1 PBPK modeling approaches 16

1.6.2 Software for PBPK modeling 17

1.6.2.1 MATLAB® and STELLA® 17

1.6.2.2 Commercial software (Simcyp®, GastroPlus®, PK-Sim®) and GI-Sim® 18

1.7 Aims of this work 20

2 Materials and Methods 21

2.1 Materials 21

2.1.1 Chemicals 21

2.1.2 Model substance cinnarizine 22

2.1.3 Model substance atazanavir 24

2.2 Methods 28

2.2.1 HPLC-UV setup 28

2.2.2 Biorelevant media 29

2.2.3 Solubility assessment 31

2.2.4 Dissolution experiments 33

2.2.5 “Dumping” experiments 33

2.2.6 Transfer experiments 33

2.2.7 WinNonLin® - assessment of pharmacokinetics of API formulations 38

2.2.8 STELLA® 39

2.2.9 Simcyp® 47

2.2.10 Statistical comparison of predicted plasma profiles using different transfer experiment approaches 51

3 Results 52
3.1 Cinnarizine – investigation of *in vitro* behavior 52
3.1.1 Solubility results 52
3.1.2 Dissolution of cinnarizine tablets in biorelevant media 53
3.1.3 Dumping of pure cinnarizine 57
3.1.4 Investigation of supersaturation and precipitation of cinnarizine during transfer experiments 58
3.2 Cinnarizine - *in silico* plasma profile simulation 66
3.2.1 Evaluation of distribution and elimination kinetics of various cinnarizine tablets using WinNonLin® 66
3.2.2 STELLA® model - investigation of permeability restrictions of cinnarizine using fed state simulations 67
3.2.3 STELLA® "dissolution-only" vs. "supersaturation and precipitation" PBPK model in cinnarizine fasted state simulations 69
3.2.4 STELLA® statistical comparison analysis of different transfer rates 73
3.2.5 STELLA® sensitivity analysis of cinnarizine plasma profile predictions 74
3.2.6 Summary of cinnarizine plasma profile simulations using Simcyp® 77
3.3 Summary of the cinnarizine investigation and formulation suggestions 78
3.4 Atazanavir sulfate – investigation of *in vitro* behavior 80
3.4.1 Solubility results 80
3.4.1.1 Equilibrium solubility 80
3.4.1.2 Kinetic solubility 82
3.4.2 Dissolution results of atazanavir sulfate capsules in biorelevant media 83
3.4.3 Dumping results of atazanavir sulfate 87
3.4.4 Investigation of the atazanavir sulfate concentration profile during simulated transfer from the stomach to the intestine 88
3.5 Atazanavir sulfate - *in silico* plasma profile simulation 95
3.5.1 Evaluation of distribution and elimination kinetics of atazanavir using WinNonLin® analysis of literature PK data 95
3.5.2 Permeability evaluation of atazanavir 96
3.5.3 STELLA® plasma profile predictions of atazanavir capsules in the fasted state 97
3.5.4 STELLA® sensitivity analysis on atazanavir plasma profile predictions 104
3.6 Summary of atazanavir plasma profile simulations using Simcyp® 109
3.7 Summary of the atazanavir investigation and formulation suggestions 110

4 General discussion and conclusions 113
4.1 Choosing the right *in vitro* investigation approach 113
4.2 Formulation enhancement approaches for weakly basic drugs 120
4.3 Choosing the right PBPK modeling approach 122
4.3.1 Development and evolution of the STELLA® model 122

4.3.2 Self-built versus commercial PBPK models (STELLA® versus Simcyp®) 123
4.3.2.1 Input of release and dissolution profiles 124
4.3.2.2 Opportunities for simulating pharmacokinetics of modified release formulations 125
4.3.2.3 Input of permeability 125
4.3.2.4 Middle-out and Bottom-up modeling approaches 126
4.3.2.5 Virtual populations 127
4.3.2.6 Summary 127
4.4 Outlook 128

5 Summary 131

6 German Summary (Deutsche Zusammenfassung) 137

7 Appendix 143
7.1 STELLA® sensitivity analysis of cinnarizine plasma profile predictions 143
7.2 STELLA® sensitivity analysis of atazanavir sulfate plasma profile predictions 145
7.3 Simcyp® plasma profile predictions of cinnarizine 148
7.3.1 Simcyp® plasma profile predictions of cinnarizine in the fasted state 148
7.3.2 Simcyp® plasma profile predictions of cinnarizine in the fed state 155
7.3.3 Simcyp® sensitivity analysis of cinnarizine plasma profile predictions 161
7.3.4 Simcyp® plasma profile predictions of cinnarizine using fitted Vd 172
7.4 Simcyp® plasma profile predictions of atazanavir 176
7.4.1 Simcyp® plasma profile predictions of atazanavir in the fasted state 176
7.4.2 Simcyp® plasma profile predictions of atazanavir in the fed state 184
7.4.3 Simcyp® sensitivity analysis of atazanavir plasma profile predictions 188

8 References 203

9 Curriculum Vitae 216
9.1 Personal Information 216
9.2 Professional experience 216
9.3 Education 217

10 Scientific Publications 218
10.1 Papers 218
10.2 Posters 218

11 Academic Teachers 218

List of Figures

Fig. 1.1: Dosage form and drug transit in the upper GI tract 3
Fig. 1.2: Categorization of APIs based on the biopharmaceutics classification system 4
Fig. 1.3: Categorization of APIs based on biopharmaceutics drug disposition classification system 6
Fig. 1.4: Characterization of APIs based on developability classification system. Green bars describe the extension of the dose solubility ratio from 250 ml to 500 ml. 7
Fig. 1.5: pH solubility behavior of weak bases and acids in relation to the upper GI pH 8
Fig. 1.6: Possible dissolution scenarios for weak bases upon entering the upper small intestine 9
Fig. 1.7: Transfer model for the *in vitro* simulation of gastric emptying 13
Fig. 2.1: Structure of cinnarizine 23
Fig. 2.2: Structure of atazanavir sulfate 26
Fig. 2.3: Evaluation of fraction of drug dissolved (f_d) and precipitation kinetics during and after gastric emptying (k_p). Total mass of drug emptied into intestine at time *t* is shown as a theoretical concentration curve (··). The observed percentage (mass) of drug dissolved in the intestine at time *t* and drug precipitation at times after gastric emptying is complete, *t',* are presented in the continuous curve (**–**). The vertical line (--) represents the time at which gastric emptying is complete, *t'* 37
Fig. 2.4: Pharmacokinetic model used in WinNonLin®: k_{01}: absorption kinetics constant, k_{10}: elimination kinetics constant, k_{12}: deep compartment inflow constant (optional), k_{21}: deep compartment outflow constant (optional). 38
Fig. 2.5: PBPK model for *in vivo* API formulation behavior, in which only dissolution is accounted for (dissolution-only PBPK model). 39
Fig. 2.6: PBPK model for *in vivo* API formulation behavior, in which dissolution, supersaturation, subsequent precipitation and efflux/extraction kinetics can be accounted for (supersaturation and precipitation PBPK model). 40
Fig. 2.7: STELLA® dissolution-only PBPK model without permeability restrictions; green: pre-absorptive kinetics (gastric and intestinal dissolution, gastric emptying), orange: post-absorptive kinetics (distribution and elimination), dotted square: (optional) deep compartment kinetics. 41
Fig. 2.8: STELLA® dissolution-only PBPK model with permeability restrictions; green: pre-absorptive kinetics (gastric and intestinal dissolution, gastric emptying), orange: post-absorptive kinetics (distribution and elimination), red: absorption kinetics, dotted square: (optional) deep compartment kinetics. 43
Fig. 2.9: STELLA® supersaturation and precipitation PBPK model with permeability restrictions; yellow: fractioning of dissolved and solid drug during gastric emptying, blue: precipitation, dissolution and re-dissolution of drug after gastric emptying, red: absorption kinetics, orange: post-absorptive kinetics (distribution and elimination), dotted square: (optional) deep compartment kinetics. 46
Fig. 3.1: Solubilities of cinnarizine in biorelevant media (logarithmic scaling). Solubility values in µg/ml along with the standard errors are shown on the bar for each medium. 53
Fig. 3.2: Dissolution of pure cinnarizine and cinnarizine tablets in fasted state gastric (A) and intestinal (B) media (some symbols are bigger than the standard deviation bars): Arlevert® (●) and Stugeron®

(■), cinnarizine 20 mg (○) and 25 mg (□) (curves are overlapping) along with the theoretical % dissolved for 20 mg cinnarizine in FaSSIF-V2, based on its solubility (- -). 55
Fig. 3.3: Dissolution of pure cinnarizine and cinnarizine tablets in the fed gastric (A) and intestinal (B) biorelevant media (some symbols are bigger than the standard deviation bars): Arlevert® (●) and Cinnarizine 30 mg tablets (▲), pure cinnarizine 20 mg (○) and 30 mg (△) along with the maximum theoretical % dissolved for 30 mg cinnarizine in FeSSGF pH 5.0, based on its solubility (- -). 56
Fig. 3.4: Concentration profile of cinnarizine after dumping a solution of 20 mg cinnarizine in 250 ml FaSSGF pH 2.0 into 500 ml FaSSIF-V2(PO_4) along with the maximum theoretical % dissolved for 20 mg cinnarizine based on its solubility in the combination of FaSSGF pH 2.0 and FaSSIF-V2(PO_4) in the ratio of 1:2 (- -). 58
Fig. 3.5: Fasted state transfer of a solution of 20 (◆), 40 (■) and 80 mg (▲) cinnarizine in FaSSGF pH 2.0 into FaSSIF-V2(PO_4) using transfer rates of 3 h^{-1} (A), 9 ml/min (B), 4 ml/min (C) and 0.5 ml/min (D). The theoretical transfer curve (**- -**) is displayed along with the maximum theoretical % dissolved for 20 mg cinnarizine based on its solubility in the combination of FaSSGF pH 2.0 and FaSSIF-V2(PO_4) in the ratio of 1:2 (– –). 59
Fig. 3.6: Fasted state transfer of 20 mg cinnarizine as a solution (●), dissolved Arlevert® tablets (◆) and intact Arlevert® tablets (▲) in FaSSGF pH 2.0 into FaSSIF-V2(PO_4) using transfer rates of 3 h^{-1} (A), 9 ml/min (B) and 4 ml/min (C). The theoretical transfer curve (**- -**) is displayed along with the maximum theoretical % dissolved for 20 mg cinnarizine based on its solubility in the combination of FaSSGF pH 2.0 and FaSSIF-V2(PO_4) in the ratio of 1:2 (– –). 61
Fig. 3.7: Fasted state transfer of Arlevert® (○) and Stugeron® (●) cinnarizine tablets at 3 h^{-1} (A), 9 ml/min (B), 4 ml/min (C) and 0.5 ml/min (D) transfer rates. The theoretical transfer curve (**- -**) is displayed along with the solubility (**– –**) of 25 mg cinnarizine in the combination of FaSSGF pH 2.0 and FaSSIF-V2(PO_4) in the ratio 1:2. 63
Fig. 3.8: Fed state transfer of Cinnarizine 30 mg tablets using the zero order transfer rate of 2 ml/min along with the theoretical transfer curve (**- -**). 65
Fig. 3.9: Fed state plasma profile predictions of Arlevert® (A) and Cinnarizine 30 mg (B) tablets using the dissolution-only PBPK models with and without permeability restrictions based on Caco-2 data. . 69
Fig. 3.10: Fasted state plasma profile predictions of Arlevert® (A) and Stugeron® (B) tablets using the dissolution–only and supersaturation and precipitation (obtained from transfer experiments at a rate of 3 h^{-1}) PBPK model. 71
Fig. 3.11: Fasted state plasma profile predictions of Arlevert® (–) and Stugeron® (–) tablets using the supersaturation and precipitation PBPK model after implementing results of different transfer rates. The *in vivo* plasma profiles of Arlevert® (○) and Stugeron® (●) are displayed against profile predictions for each transfer rate, i.e. 3 h^{-1} (A), 9 ml/min (B), 4 ml/min (C) and 0.5 ml/min (D). 74
Fig. 3.12: Arlevert® in the fasted state - sensitivity analysis of the fraction dissolved constant (A), precipitation constant (B), the gastric emptying rate (C) and the effective permeability (D) on cinnarizine plasma profiles..... 75

Fig. 3.13: Arlevert® in the fed state - sensitivity analysis of the z value in FeSSGF (A), the z value in FeSSIF-V2 (B) the gastric emptying rate (C) and the effective permeability (D) on cinnarizine plasma profiles 76
Fig. 3.14: Equilibrium solubilities of atazanavir in biorelevant media (logarithmic scaling). Solubility values in µg/ml along with the standard deviations are shown on the bar for each medium (n=3). 82
Fig. 3.15: Kinetic solubilities of atazanavir sulfate in biorelevant media over 24 hours (some symbols are bigger than the standard deviation bars) (n=3). 83
Fig. 3.16: Dissolution of different doses of atazanavir sulfate capsules (Reyataz®) in fasted state gastric (A) and intestinal (B) media (symbols are bigger than the standard deviation bars): 100 mg (◆), 200 mg (■), 400 mg (▲), 1200 mg (●) and solubility (- -). 84
Fig. 3.17: Dissolution of 400 mg atazanavir sulfate capsules (Reyataz®) in the fed state biorelevant media (some symbols are bigger than the standard deviation bars): FeSSGEm pH 2.75 (▲) and FeSSGEm pH 5.0 (■) along with the equilibrium solubility in FeSSGEm pH 2.75 (--) and in FeSSGEm pH 5.0 (– –). Concentrations are presented in a logarithmic scale. 85
Fig. 3.18: Dissolution of 400 mg atazanavir sulfate capsules (Reyataz®) in FeSSIF-V2 (◆) (some symbols are bigger than the standard deviation bars) along with the equilibrium solubility (--). Symbols are bigger than the standard deviation bars. 86
Fig. 3.19: Concentration profile of 200 mg atazanavir after the pre-dissolved compound in 250 ml FaSSGF pH 2.0 into 500 ml of FaSSIF-V2(PO_4) (some symbols are bigger than the standard deviation bars). The dotted line represents the kinetic solubility relative to the 200 mg atazanavir dose. 88
Fig. 3.20: Simulated fasted state transfer results of 100 mg (◆) and 200 mg (■) pre-dissolved atazanavir sulfate using the zero order transfer rate of 9 ml/min. The kinetic solubilities of atazanavir sulfate (solubility value at hour 1 in the 1:2 FaSSGF pH 2.0/FaSSIF-V2(PO_4) mixture) relative to the corresponding dose (– –) are presented along with the theoretical transfer curve (- -). Some of the error bars are smaller than the symbols. 89
Fig. 3.21: Simulated fasted state transfer results of Reyataz® 200 mg (amorphous) (▲), 200 mg atazanavir sulfate compound (crystalline) (○) and pre-dissolved 200 mg atazanavir sulfate (crystalline) (□) using the zero order transfer rate of 9 ml/min. The kinetic solubility of atazanavir sulfate (solubility value at hour 1 in the 1:2 FaSSGF pH 2.0/FaSSIF-V2(PO_4) mixture) relative to the 200 mg dose (– –) is presented along with the theoretical transfer curve (- -). Some of the error bars are smaller than the symbols. 90
Fig. 3.22: Simulated fasted state transfer results of atazanavir sulfate capsules 100 mg (◆), 200 mg (■), 400 mg (▲), 1200 mg (●) using the first order transfer of 4 h^{-1} (A) and zero order transfer rates of 9 ml/min (B) and 2 ml/min (C). The kinetic solubilities of atazanavir sulfate (solubility value at hour 1 in the 1:2 FaSSGF pH 2.0/FaSSIF-V2(PO_4) mixture) relative to the corresponding dose (– –) are presented along with the theoretical transfer curve (**- -**). Some of the error bars are smaller than the symbols. 91
Fig. 3.23: Simulated fed state transfer results of 400 mg (2 x 200 mg) Reyataz® capsules using the 4 ml/min zero order transfer rate for 250 ml of FeSSGEm pH 2.75 (△) and FeSSGF pH 2.75 (▲) as a

donor compartment. The solubilities of atazanavir sulfate in mixtures of FeSSGEm pH 2.75/FeSSIF-V2 (1:2) (– -) and FeSSGF pH 2.75/FeSSIF-V2 (1:2) (– –) are presented along with the theoretical transfer curve (- -). Some of the error bars are smaller than the symbols. 93
Fig. 3.24: Fed state transfer results (simulating the high fat meal) of 400 mg (2 x 200 mg) Reyataz® capsules using the 2 ml/min zero order transfer rate for 500 ml of FeSSGEm pH 5.0 (◆) as a donor compartment. The solubility of atazanavir sulfate in FeSSIF-V2 (– –) is presented along with the theoretical transfer curve (- -). Error bars are smaller than the symbols..... 93
Fig. 3.25: Observed (●) and predicted fasted state plasma profiles of 100 mg atazanavir sulfate capsules with 90% (–) and without (- -) efflux/extraction kinetics. Coefficient of variation is shown for the C_{max} value (reported as geometric mean (□)). 99
Fig. 3.26: Observed (●) and predicted fasted state plasma profiles of 200 mg (A), 400 mg (B) and 1200 mg (C) atazanavir sulfate capsules (**–**). Coefficients of variation are shown for the C_{max} values (reported as geometric means (□)). 100
Fig. 3.27: Observed and predicted fed state plasma profiles of 400 mg atazanavir sulfate (2 x 200 mg Reyataz®) capsules. Predictions were made using different transfer experiments using either FeSSGF pH 2.75 (“best case”) or FeSSGEm pH 2.75 (“worst case”) as donor media. The solid line shows the average of the best and worst case scenarios..... 103
Fig. 3.28: Sensitivity analysis of the fraction dissolved constant < 5 min (A), the fraction dissolved constant > 5 min (B), the gastric emptying constant (C), the permeability (D) the volume of distribution (E), and the elimination constant (F) on plasma profile predictions of 400 mg (2 x 200 mg) atazanavir sulfate capsules in the fasted state. The observed *in vivo* profile is shown along with coefficient of variation for the C_{max} value (reported as geometric mean). 105
Fig. 3.29: Sensitivity analysis was performed for simulations using data obtained from transfer experiments with FeSSGEm pH 2.75 as the donor compartment (“worst case”). Analysis of the fraction dissolved constant < 10 min (A), the fraction dissolved constant > 10 min (B), the precipitation constant (C), the gastric emptying constant (D), the permeability (E), the elimination constant (F), and the volume of distribution (G) on plasma profile predictions of 400 mg (2 x 200 mg) atazanavir sulfate in the fed state. 107
Fig. 3.30: Sensitivity analysis was performed for simulations using data obtained from transfer experiments with FeSSGF pH 2.75 as the donor compartment (“best case”). Analysis of the fraction dissolved constant < 20 min (A), the fraction dissolved constant > 20 min (B), the gastric emptying constant (C), the permeability (D), the volume of distribution (E) and the elimination constant (F) on plasma profile predictions of 400 mg (2 x 200 mg) atazanavir sulfate in the fed state. 108
Fig. 4.1: Proposed outline of *in vitro* experiments for investigation and development of drug products containing weak bases..... 115
Fig. 4.2: Coupling of *in vitro* data to *in silico* PBPK/PD modeling in order to investigate a therapeutic outcome of an API. 129
Fig. 7.1: Stugeron® in the fasted state - sensitivity analysis of the fraction dissolved constant (A), the precipitation constant (B), the gastric emptying rate (C) and the effective permeability (D) on cinnarizine plasma profiles..... 143

Fig. 7.2: Cinnarizine 30 mg tablets in the fed state - sensitivity analysis of the z value in FeSSGF (A), the z value in FeSSIF-V2 (B) the gastric emptying rate (C) and the effective permeability (D) on cinnarizine plasma profiles. 144
Fig. 7.3: Sensitivity analysis of the fraction dissolved constant < 5 min (A), the fraction dissolved constant > 5 min (B), the gastric emptying constant (C), the permeability (D), the volume of distribution (E), and the elimination constant (F) on plasma profile predictions of 100 mg atazanavir sulfate capsules in the fasted state. 145
Fig. 7.4: Sensitivity analysis of the fraction dissolved constant < 5 min (A), the fraction dissolved constant > 5 min (B), the gastric emptying constant (C), the permeability (D), the volume of distribution (E), and the elimination constant (F) on plasma profile predictions of 200 mg atazanavir sulfate capsules in the fasted state. 146
Fig. 7.5: Sensitivity analysis of the fraction dissolved constant (A), the first order precipitation constant (B), the gastric emptying constant (C), the permeability (D), the volume of distribution (E), and the elimination constant (F) on plasma profile predictions of 1200 mg atazanavir sulfate capsules in the fasted state. 147
Fig. 7.6: Fasted state plasma profile predictions of Arlevert® 20 mg (A) and Stugeron® 25 mg (B) by implementing biorelevant solubility of cinnarizine into the Simcyp® gastrointestinal solubility mask. . 149
Fig. 7.7: Fasted state plasma profile predictions of Arlevert® 20 mg (A) and Stugeron® 25 mg (B) using Simcyp® predictions of cinnarizine solubility based on its physicochemical properties. 152
Fig. 7.8: pH solubility profile of cinnarizine predicted by Simcyp®. 152
Fig. 7.9: Fasted state plasma profile predictions of Arlevert® 20 mg (A) and Stugeron® 25 mg (B) by implementing cinnarizine solubility at different pH values into the Simcyp® mask. 154
Fig. 7.10: Fed state plasma profile predictions of Arlevert® 20 mg (A) and Cinnarizine 30 mg tablets (B) by implementing dissolution profiles in FeSSGF pH 5.0 and FeSSIF-V2 into Simcyp®. 156
Fig. 7.11: Fed state plasma profile predictions of Arlevert® 20 mg (A) and Cinnarizine 30 mg tablets (B) by implementing biorelevant solubility of cinnarizine into the Simcyp® gastrointestinal solubility mask. 158
Fig. 7.12: Fed state plasma profile predictions of Arlevert® 20 mg (A) and Cinnarizine 30 mg tablets (B) using Simcyp® predictions of cinnarizine solubility based on its physicochemical properties. 159
Fig. 7.13: Fed state plasma profile predictions of Arlevert® 20 mg (A) and Cinnarizine 30 mg tablets (B) by implementing cinnarizine solubility at different pH values into the Simcyp® mask. 161
Fig. 7.14: Sensitivity analysis of the gastric emptying (A), the permeability (B), the volume of distribution (C) and the clearance (D) on plasma profile predictions of Arlevert® in the fed state by implementing dissolution profiles in FeSSGF pH 5.0 and FeSSIF-V2 into Simcyp®. 162
Fig. 7.15: Sensitivity analysis of the gastric emptying (A), the permeability (B), the volume of distribution (C) and the clearance (D) on plasma profile predictions of Cinnarizine 30 mg tablets in the fed state by implementing dissolution profiles in FeSSGF pH 5.0 and FeSSIF-V2 into Simcyp®. 163
Fig. 7.16: Sensitivity analysis of the intestinal solubility (A), the supersaturation (B), the precipitation (C), the gastric emptying (D), the permeability (E), the volume of distribution (F) and the clearance (G)

on plasma profile predictions of Arlevert® in the fasted state by implementing biorelevant solubility of cinnarizine into the Simcyp® gastrointestinal solubility mask. 164
Fig. 7.17: Sensitivity analysis of the intestinal solubility (A), the supersaturation (B), the precipitation (C), the gastric emptying (D), the permeability (E), the volume of distribution (F) and the clearance (G) on plasma profile predictions of Stugeron® in the fasted state by implementing biorelevant solubility of cinnarizine into the Simcyp® gastrointestinal solubility mask. 165
Fig. 7.18: Sensitivity analysis of the gastric solubility (A), the intestinal solubility (B), the gastric emptying (C), the permeability (D), the volume of distribution (E) and the clearance (F) on plasma profile predictions of Arlevert® in the fed state by implementing biorelevant solubility of cinnarizine into the Simcyp® gastrointestinal solubility mask. 167
Fig. 7.19: Sensitivity analysis of the gastric solubility (A), the intestinal solubility (B), the gastric emptying (C), the permeability (D), the volume of distribution (E) and the clearance (F) on plasma profile predictions of Cinnarizine 30 mg tablets in the fed state by implementing biorelevant solubility of cinnarizine into the Simcyp® gastrointestinal solubility mask. 168
Fig. 7.20: Sensitivity analysis of the supersaturation (A), the precipitation (B), the gastric emptying (C), the permeability (D), the volume of distribution (E) and the clearance (F) on plasma profile predictions of Arlevert® in the fasted state using Simcyp® predictions of cinnarizine solubility by based on its physicochemical properties. 169
Fig. 7.21: Sensitivity analysis of the supersaturation (A), the precipitation (B), the gastric emptying (C), the permeability (D), the volume of distribution (E) and the clearance (F) on plasma profile predictions of Stugeron® in the fasted state using Simcyp® predictions of cinnarizine solubility based on its physicochemical properties. 170
Fig. 7.22: Sensitivity analysis of the gastric emptying (A), the permeability (B), the volume of distribution (C) and the clearance (D) on plasma profile predictions of Arlevert® in the fed state using Simcyp® predictions of cinnarizine solubility based on its physicochemical properties. 171
Fig. 7.23: Sensitivity analysis of the gastric emptying (A), the permeability (B), the volume of distribution (C) and the clearance (D) on plasma profile predictions of Cinnarizine 30 mg tablets in the fed state using Simcyp® predictions of cinnarizine solubility based on its physicochemical properties. 172
Fig. 7.24: Fasted state plasma profile predictions of Arlevert® 20 mg (A) and Stugeron® 25 mg (B) by implementing biorelevant solubility of cinnarizine into the Simcyp® gastrointestinal solubility mask. The two profiles were simulated using the “old Vd” (–) and “new Vd” (--) values. 173
Fig. 7.25: Fed state plasma profile predictions of Arlevert® 20 mg (A) and Cinnarizine 30 mg tablets (B) by implementing biorelevant dissolution profiles into the Simcyp® mask. The two profiles were simulated using the “old Vd” (–) and “new Vd” (--) values. 175
Fig. 7.26: Fasted state plasma profile predictions of atazanavir sulfate 100 mg (A), 200 mg (B), 400 mg (C) and 1200 mg (D) capsules by implementing kinetic biorelevant solubility of atazanavir into the Simcyp® gastrointestinal solubility mask. 178
Fig. 7.27: Predicted pH solubility profile for atazanavir in Simcyp®. 180

Fig. 7.28: Fasted state plasma profile predictions of atazanavir sulfate 100 mg (A), 200 mg (B), 400 mg (C) and 1200 mg (D) capsules using Simcyp® predictions of atazanavir solubility based on its physicochemical properties. 180
Fig. 7.29: Fasted state plasma profile predictions of atazanavir sulfate 100 mg (A), 200 mg (B), 400 mg (C) and 1200 mg (D) capsules by implementing equilibrium solubilities of atazanavir at different pH values into the Simcyp® mask. 182
Fig. 7.30: Fed state plasma profile predictions of atazanavir sulfate 400 mg capsules (2 x 200 Reyataz®) by implementing biorelevant solubility data into the Simcyp® gastrointestinal solubility mask: “worst case” (--) (using FeSSGEm pH 2.75 data) and “best case” (– –) (using FeSSGF pH 2.75 data). 184
Fig. 7.31: Fed state plasma profile predictions of atazanavir sulfate 400 mg capsules (2 x 200 Reyataz®) by using Simcyp® predictions of atazanavir solubility based on its physicochemical properties: “worst case” (--) (using FeSSGEm pH 2.75 data) and “best case” (– –) (using FeSSGF pH 2.75 data). 186
Fig. 7.32: Fed state plasma profile predictions of atazanavir sulfate 400 mg capsules (2 x 200 Reyataz®) by implementing equilibrium solubilities of atazanavir at different pH values into the Simcyp® mask: “worst case” (--) (using FeSSGEm pH 2.75 data) and “best case” (– –) (using FeSSGF pH 2.75 data). 187
Fig. 7.33: Sensitivity analysis of the intestinal solubility (A), the gastric emptying (B), the permeability (C), the volume of distribution (D) and the clearance (E) on plasma profile predictions of 100 mg atazanavir sulfate in the fasted state by implementing biorelevant solubility of atazanavir into the Simcyp® gastrointestinal solubility mask. 189
Fig. 7.34: Sensitivity analysis of the intestinal solubility (A), the gastric emptying (B), the permeability (C), the volume of distribution (D) and the clearance (E) on plasma profile predictions of 200 mg atazanavir sulfate in the fasted state by implementing biorelevant solubility of atazanavir into the Simcyp® gastrointestinal solubility mask. 190
Fig. 7.35: Sensitivity analysis of the intestinal solubility (A), the gastric emptying (B), the permeability (C), the volume of distribution (D) and the clearance (E) on plasma profile predictions of 400 mg atazanavir sulfate in the fasted state by implementing biorelevant solubility of atazanavir into the Simcyp® gastrointestinal solubility mask. 191
Fig. 7.36: Sensitivity analysis of the intestinal solubility (A), the gastric emptying (B), the permeability (C), the volume of distribution (D) and the clearance (E) on plasma profile predictions of 1200 mg atazanavir sulfate in the fasted state by implementing biorelevant solubility of atazanavir into the Simcyp® gastrointestinal solubility mask. 192
Fig. 7.37: “worst case” example - sensitivity analysis of the intestinal solubility (A), the supersaturation (B), the precipitation (C), the gastric emptying (D), the permeability (E), the volume of distribution (F) and the clearance (G) on plasma profile predictions of 400 mg atazanavir sulfate in the fed state by implementing biorelevant solubility of atazanavir into the Simcyp® gastrointestinal solubility mask... 193
Fig. 7.38: “best case” example - sensitivity analysis of the intestinal solubility (A), the gastric emptying (B), the permeability (C), the volume of distribution (D) and the clearance (E) on plasma profile

predictions of 400 mg atazanavir sulfate in the fed state by implementing biorelevant solubility of atazanavir into the Simcyp® gastrointestinal solubility mask. 194
Fig. 7.39: Sensitivity analysis of the gastric emptying (A), the permeability (B), the volume of distribution (C) and the clearance (D) on plasma profile predictions of 100 mg atazanavir sulfate in the fasted state using predicted atazanavir solubility by Simcyp®. 195
Fig. 7.40: Sensitivity analysis of the gastric emptying (A), the permeability (B), the volume of distribution (C) and the clearance (D) on plasma profile predictions of 200 mg atazanavir sulfate in the fasted state using predicted atazanavir solubility by Simcyp®. 195
Fig. 7.41: Sensitivity analysis of the gastric emptying (A), the permeability (B), the volume of distribution (C) and the clearance (D) on plasma profile predictions of 400 mg atazanavir sulfate in the fasted state using predicted atazanavir solubility by Simcyp®. 196
Fig. 7.42: Sensitivity analysis of the gastric emptying (A), the permeability (B), the volume of distribution (C) and the clearance (D) on plasma profile predictions of 1200 mg atazanavir sulfate in the fasted state using predicted atazanavir solubility by Simcyp®. 196
Fig. 7.43: “worst case” example - sensitivity analysis of supersaturation (A), precipitation (B), the gastric emptying (C), the permeability (D), the volume of distribution (E) and the clearance (F) on plasma profile predictions of 400 mg atazanavir sulfate in the fed state using predicted atazanavir solubility by Simcyp®. 197
Fig. 7.44: “best case” example - sensitivity analysis of the gastric emptying (A), the permeability (B), the volume of distribution (C) and the clearance (D) on plasma profile predictions of 400 mg atazanavir sulfate in the fed state using predicted atazanavir solubility by Simcyp® 198
Fig. 7.45: Sensitivity analysis of the gastric emptying (A), the permeability (B), the volume of distribution (C) and the clearance (D) on plasma profile predictions of 200 mg atazanavir sulfate in the fasted state by implementing equilibrium solubilities of atazanavir at different pH values into the Simcyp® mask. 199
Fig. 7.46: Sensitivity analysis of the gastric emptying (A), the permeability (B), the volume of distribution (C) and clearance (D) on plasma profile predictions of 200 mg atazanavir sulfate in the fasted state by implementing equilibrium solubilities of atazanavir at different pH values into the Simcyp® mask. 199
Fig. 7.47: Sensitivity analysis of the gastric emptying (A), the permeability (B), the volume of distribution (C) and the clearance (D) on plasma profile predictions of 400 mg atazanavir sulfate in the fasted state by implementing equilibrium solubilities of atazanavir at different pH values into the Simcyp® mask. 200
Fig. 7.48: Sensitivity analysis of the gastric emptying (A), the permeability (B), the volume of distribution (C) and the clearance (D) on plasma profile predictions of 1200 mg atazanavir sulfate in the fasted state by implementing equilibrium solubilities of atazanavir at different pH values into the Simcyp® mask. 200
Fig. 7.49: “worst case” example - sensitivity analysis of the supersaturation (A), the precipitation (B), the gastric emptying (C), the permeability (D), the volume of distribution (E) and the clearance (F) on

plasma profile predictions of 400 mg atazanavir sulfate in the fed state by implementing equilibrium solubilities of atazanavir at different pH values into the Simcyp® mask. 201
Fig. 7.50: “best case” example - sensitivity analysis of the gastric emptying (A), the permeability (B), the volume of distribution (C) and the clearance (D) on plasma profile predictions of 400 mg atazanavir sulfate in the fed state by implementing equilibrium solubilities of atazanavir at different pH values into the Simcyp® mask. 202

List of Tablets

Table 2.1: HPLC setup for the analysis of cinnarizine and atazanavir 28
Table 2.2: Composition of the biorelevant media simulating gastric fasted state 30
Table 2.3: Composition of the biorelevant media simulating gastric fed state 30
Table 2.4: Composition of the biorelevant media simulating gastric fed state under light meal conditions with orange juice 31
Table 2.5: Composition of the biorelevant media simulating fasted and fed intestinal states 31
Table 2.6: Pre-absorptive parameters (fasted and fed state) used in STELLA® PBPK models 43
Table 2.7: Pre-absorptive parameters (fasted and fed state) used in the Simcyp® modeling mask 48
Table 3.1: Initial dissolution rates (z values) for the various biorelevant media and cinnarizine formulations 57
Table 3.2: Maximum supersaturation ratios (maximum concentration achieved in the acceptor compartment relative to the solubility) of different doses of cinnarizine at various transfer rates 60
Table 3.3 First order precipitation constants of different doses of cinnarizine at various transfer rates 60
Table 3.4: Maximum supersaturation ratios (maximum concentration achieved in the acceptor compartment relative to the solubility) of different presentations of 20 mg cinnarizine at various transfer rates 62
Table 3.5: First order precipitation constants of different presentations of 20 mg cinnarizine at various transfer rates 62
Table 3.6: Maximum supersaturation ratios, fraction dissolved (f_d) and precipitation constants (k_p) for Arlevert® and Stugeron® for different transfer rates. 64
Table 3.7: Pre-absorptive and absorptive parameters needed for the plasma profile simulation of cinnarizine using STELLA® 67
Table 3.8: Distribution and elimination parameters of cinnarizine used for *in silico* simulations (STELLA® and Simcyp®) 67
Table 3.9: Comparison of *in vivo* data with *in silico* predictions of different PBPK models for Arlevert®, Cinnarizine 30 mg tablets and Stugeron® in the fasted and fed state 72
Table 3.10: Statistical comparison of *in silico* predictions to *in vivo* observations using the difference factor (f_1) and point estimate ratios of bioequivalence test parameters for different cinnarizine IR formulations and transfer experiments (best fits in boldface). 73
Table 3.11: pH values in the dissolution vessel after dissolution of different doses of atazanavir sulfate in FaSSIF-V2 85
Table 3.12: Initial dissolution rates (z values) for the various biorelevant media and Reyataz® doses 86
Table 3.13: Maximum supersaturation ratios, fraction dissolved (f_d) and precipitation (k_p) constants of different doses of atazanavir sulfate (Reyataz®) for different simulated gastrointestinal states 94
Table 3.14: Distribution and elimination parameters of atazanavir used for *in silico* simulations (STELLA® and Simcyp®) 96

Table 3.15: Pre-absorptive and absorptive parameters needed for the plasma profile simulation of atazanavir using STELLA® 97
Table 3.16: *In vivo* and predicted pharmacokinetic parameters for different doses of atazanavir sulfate in the fasted state 101
Table 3.17: *In vivo* and predicted pharmacokinetic parameters for 400 mg atazanavir sulfate (2 x 200 mg Reyataz®) capsules in the fed state 104
Table 7.1: Standard physicochemical parameters of cinnarizine implemented into Simcyp® 148
Table 7.2: *In vivo* and predicted pharmacokinetic parameters for Arlevert® and Stugeron® tablets in the fasted state by implementing biorelevant solubility of cinnarizine into the Simcyp® gastrointestinal solubility mask 149
Table 7.3: Ratios of predicted (using the GI solubility approach) to observed plasma profile parameters of cinnarizine tablets in the fasted state 150
Table 7.4 *In vivo* and predicted pharmacokinetic parameters for Arlevert® and Stugeron® tablets in the fasted state using Simcyp® predictions of cinnarizine solubility based on its physicochemical properties. 151
Table 7.5: *In vivo* and predicted pharmacokinetic parameters for Arlevert® and Stugeron® tablets in the fasted state by implementing cinnarizine solubility at different pH values into the Simcyp® mask 154
Table 7.6: *In vivo* and predicted pharmacokinetic parameters for Arlevert® and Cinnarizine 30 mg tablets in the fed state by implementing dissolution profiles in FeSSGF pH 5.0 and FeSSIF-V2 into Simcyp® 155
Table 7.7: Ratios of predicted (using dissolution profile data) to observed plasma profile parameters of cinnarizine tablets in the fed state 157
Table 7.8: *In vivo* and predicted pharmacokinetic parameters for Arlevert® and Cinnarizine 30 mg tablets in the fed state by implementing biorelevant solubility of cinnarizine into the Simcyp® gastrointestinal solubility mask 157
Table 7.9: *In vivo* and predicted pharmacokinetic parameters for Arlevert® and Cinnarizine 30 mg tablets in the fed state using Simcyp® predictions of cinnarizine solubility based on its physicochemical properties 159
Table 7.10: *In vivo* and predicted pharmacokinetic parameters for Arlevert® and Cinnarizine 30 mg tablets in the fed state by implementing cinnarizine solubility at different pH values into the Simcyp® mask 160
Table 7.11: *In vivo* and predicted (Vd new and Vd old) pharmacokinetic parameters for Arlevert® and Stugeron® tablets in the fasted state by implementing biorelevant solubility of cinnarizine into the Simcyp® gastrointestinal solubility mask 173
Table 7.12: *In vivo* and predicted (Vd new and Vd old) pharmacokinetic parameters for Arlevert® and Cinnarizine 30 mg tablets in the fed state by implementing dissolution profiles in FeSSGF pH 5.0 and FeSSIF-V2 into Simcyp® 174
Table 7.13: Absorption, distribution and elimination parameters of atazanavir implemented into Simcyp® 176